Late onset, sporadic Alzheimer's disease is a heterogeneous disorder (Casserly and Topol, 2004) and the contribution of a vascular factor is still controversial. In contrast to vascular-type cognitive impairment, no significant change (at most, a mild increase) in the level of circulating CD34+ cells was observed in patients with Alzheimer's-type cognitive impairment who had no cerebral ischemia. Consistent with a CD34+ cell-independent mechanism of cognitive decline in Alzheimer's-type impaired cognition, there was no correlation between circulating CD34+ cells and the level of CDR or MMSE. These results suggest that the level of CD34+ cells in the peripheral circulation might provide a useful means of separating dementia with a vascular etiology from dementia associated with nonvascular causes. This is not inconsistent with a previous report indicating decreased levels of CD34+ cells in patients with early Alzheimer's disease that did not exclude patients with coexisting cerebral ischemia (Maler *et al*, 2006). Our findings could have implications for treatment, especially as more modalities become available for patients with declining cognitive function.

The level of circulating endothelial progenitor cells, identified based on positivity for CD34 and kinase insert domain receptor (CD34+/KDR+ cells), has been correlated with cardiovascular risk factors (Vasa *et al*, 2001) and cardiovascular outcomes (Schmidt-Lucke *et al*, 2005; Werner *et al*, 2005). However, large variations in the levels of CD34+/KDR+ cells in the latter reports (by ~100-fold between reports; Fadini *et al*, 2006; Werner *et al*, 2005) indicate the need to standardize this measurement. In contrast, in our study, although there was no strong correlation between levels of CD34+ cells and established cardiovascular risk factors and other treatments, probably because of the heterogeneity of our control subjects, the results indicate a close relationship between the overall CD34+ pool and the cognitive impairment with cerebral ischemia. Previous reports have indicated a positive correlation between mobilization of CD34+ cells and improved functional outcome in stroke patients (Dunac *et al*, 2007). Accelerated functional recovery after experimental stroke, because of administration of CD34+ cells (Shyu *et al*, 2006; Taguchi *et al*, 2004*b*), suggests the possible contribution of CD34+ cells in maintenance of brain function during cerebral circulation. Our method for quantification of CD34+ cells is simple, reproducible (Kikuchi-Taura *et al*, 2006), and suitable for screening a broad group of patients at risk for cerebrovascular disorders.

In conclusion, our results indicate that the level of circulating CD34+ cells provides a marker of vascular risk associated with cognitive impairment. Furthermore, differences in the pathobiology of Alzheimer's- and vascular-type cognitive impairment may be mirrored in levels of circulating CD34+ cells in these patient populations.

Acknowledgements

We thank Y Kasahara, K Obata, and Y Okinaka for technical assistance.

Conflict of interest

The authors state no conflict of interest.

References

American Psychiatric Association (1994) *Diagnostic and statistical manual of mental disorders*. 4th ed Washington, DC: American Psychiatric Association

Asahara T, Murohara T, Sullivan A, Silver M, van der Zee R, Li T, Witzenbichler B, Schatteman G, Isner JM (1997) Isolation of putative progenitor endothelial cells for angiogenesis. *Science* 275:964–7

Casserly I, Topol E (2004) Convergence of atherosclerosis and Alzheimer's disease: inflammation, cholesterol, and misfolded proteins. *Lancet* 363:1139–46

Dunac A, Frelin C, Popolo-Blondeau M, Chatel M, Mahagne MH, Philip PJ (2007) Neurological and functional recovery in human stroke are associated with peripheral blood CD34+ cell mobilization. *J Neurol* 254:327–32

Fadini GP, Coracina A, Baesso I, Agostini C, Tiengo A, Avogaro A, de Kreutzenberg SV (2006) Peripheral blood CD34+KDR+ endothelial progenitor cells are determinants of subclinical atherosclerosis in a middle-aged general population. *Stroke* 37:2277–82

Kikuchi-Taura A, Soma T, Matsuyama T, Stern DM, Taguchi A (2006) A new protocol for quantifying CD34+ cells in peripheral blood of patients with cardiovascular disease. *Texas Heart Inst J* 33:427–9

Majka M, Janowska-Wieczorek A, Ratajczak J, Ehrenman K, Pietrzkowski Z, Kowalska MA, Gewirtz AM, Emerson SG, Ratajczak MZ (2001) Numerous growth factors, cytokines, and chemokines are secreted by human CD34(+) cells, myeloblasts, erythroblasts, and megakaryoblasts and regulate normal hematopoiesis in an autocrine/paracrine manner. *Blood* 97: 3075–85

Maler JM, Spitzer P, Lewczuk P, Kornhuber J, Herrmann M, Wiltfang J (2006) Decreased circulating CD34+ stem cells in early Alzheimer's disease: evidence for a deficient hematopoietic brain support? *Mol Psychiatry* 11:1113–5

Schmidt-Lucke C, Rossig L, Fichtlscherer S, Vasa M, Britten M, Kamper U, Dimmeler S, Zeiher AM (2005) Reduced number of circulating endothelial progenitor cells predicts future cardiovascular events: proof of concept for the clinical importance of endogenous vascular repair. *Circulation* 111:2981–7

Shyu WC, Lin SZ, Chiang MF, Su CY, Li H (2006) Intracerebral peripheral blood stem cell (CD34+) implantation induces neuroplasticity by enhancing beta1 integrin-mediated angiogenesis in chronic stroke rats. *J Neurosci* 26:3444–53

Sutherland DR, Anderson L, Keeney M, Nayar R, Chin-Yee I (1996) The ISHAGE guidelines for CD34+ cell determination by flow cytometry. International Society of Hematotherapy and Graft Engineering. *J Hematother* 5:213–26

Taguchi A, Matsuyama T, Moriwaki H, Hayashi T, Hayashida K, Nagatsuka K, Todo K, Mori K, Stern DM, Soma T, Naritomi H (2004*a*) Circulating CD34-positive cells provide an index of cerebrovascular function. *Circulation* 109:2972–5

Taguchi A, Soma T, Tanaka H, Kanda T, Nishimura H, Yoshikawa H, Tsukamoto Y, Iso H, Fujimori Y, Stern DM, Naritomi H, Matsuyama T (2004*b*) Administration of CD34+ cells after stroke enhances neurogenesis via angiogenesis in a mouse model. *J Clin Invest* 114: 330–8

Vagnucci Jr AH, Li WW (2003) Alzheimer's disease and angiogenesis. *Lancet* 361:605–8

Vasa M, Fichtlscherer S, Aicher A, Adler K, Urbich C, Martin H, Zeiher AM, Dimmeler S (2001) Number and migratory activity of circulating endothelial progenitor cells inversely correlate with risk factors for coronary artery disease. *Circ Res* 89:E1–7

Werner N, Kosiol S, Schiegl T, Ahlers P, Walenta K, Link A, Bohm M, Nickenig G (2005) Circulating endothelial progenitor cells and cardiovascular outcomes. *New Engl J Med* 353:999–1007

神経インターフェース

齋藤　敬

応用物理　第76巻　第12号（2007年）抜刷

研究紹介

神経インターフェース

齋藤　敬

神経細胞は生体の情報伝達配線であり，かつ演算素子である．この神経細胞と人工物の間で情報伝達を仲介するデバイスは神経インターフェースと総称される．その開発に際してはインターフェースそのもの，またインターフェースが適切に情報を伝達しているかの評価に必要な身体模擬デバイスの両方が必要になる．ここでは，個々の細胞を対象とした細胞膜せん孔法，および移動・運搬能力に特化した動物模擬ロボットの二つの要素技術について，全体の背景となる神経インターフェースとの関連を含め，技術の成り立ちや今後の展開など紹介する．

Keywords : neural interface, robot, cell membrane, oxidation, manipulator

1. まえがき

神経インターフェースとは，図1に示すように生体末端部の機能か，そこまでの情報接続に回復不能な損傷が生じた場合，生体配線部（神経）と機器配線部（データバス）を直結して人工物により機能を代行するための結合部である．

私の現在までの研究成果としては，細胞を対象とした光化学と，古典的な機械工学によって次世代神経インターフェースへの土台を築いた段階で，バイオエレクトロニクス的な発展はまったくこれからである．しかし神経インターフェースに求められるものは何か，私なりに原点から再構築した結果であり，理解いただければ幸いである．

2. 神経インターフェースの問題点

現在，神経と多くの情報授受を行いうる手段としては電極の利用が一般的であるが，実際に授受可能な情報量には大きな制約がある．情報量の制約が生ずる理由は，神経細胞と電極間の「一対一かつ双方向の情報授受」が達成できていないためである．これは神経細胞の外に計測・刺激用の電極を設置せざるを得ない点に大きな原因がある．

例えば，末梢神経においてはさまざまな入出力の配線（神経細胞の軸索部）が混在しているため，個々の神経細胞の担当信号に合わせて入出力を行わなければならない．神経細胞の細胞膜における電位変化がこの信号に相当するが，大まかにいえば，膜電位で−70 mV（OFF状態）から30 mV（ON状態）程度，信号強度により0〜300 Hzの頻度範囲で変動する一種のデジタル信号である．この信号に対し，細胞外電極では周辺の複数の神経細胞からの信号の総和しか記録できない．また計測される電位変化は数十μV〜数百μVと微弱であるために，厳重なノイズ対策が必要になる．その一方で，細胞外電極によって神経を電気刺激（強制的にON）する際には，刺激に必要なしきい値である約30 mVの膜電位変化に対し，条件にもよるがその10倍以上の電圧を電極に印加する必要がある．現在，技術上は細胞並みの集積度で電極アレイを作成可能であるが，アレイ内で計測と刺激を同時に行えば，刺激処理によって微弱な神経活動の計測はマスクされてしまうことになる．また，刺激電極周辺の細胞群を非選択的にONにしてしまう．

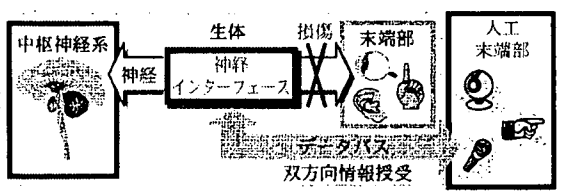

図1　神経インターフェース概略．

これに対し，細胞膜をせん孔して使用可能なガラス管微小電極[1]，パッチ電極[2]は，細胞本来の電圧・電流値に近い値で細胞膜電位・電流の計測や神経刺激が可能である．これらは細胞内電極と呼ばれるが，細胞を機械的に傷つけることになるため，細胞死を誘発しやすい．このため，既存の細胞内電極はあくまでも基礎研究用途に限られている．

重要な点として，単に鋭い構造体を細胞に接触させても細胞膜の柔軟性・流動性に阻まれ細胞膜のせん孔は困難で，無理をすると細胞を破壊してしまう問題がある．膜に対する刺入ではなく，吸引せん孔を利用するパッチ電極についてはチップ化[3]も成功している．しかし集積化については，個々の細胞と電極部の接続時にそれぞれ精密な吸引制御が必要なため，集積運用は困難という問題に直面している．その他，細胞に対する物質導入方法として，集束レーザー光による細胞膜せん孔も80年代に開発されたが[4]，その後

大阪大学 産業科学研究所　〒567-0047　茨木市美穂ヶ丘8-1．e-mail : saito@sanken.osaka-u.ac.jp　分類番号　9.4, 12.6
Neural interfaces—The cellular-level approach and living-body-mimicking robotics for their evaluation—. Takashi Kei SAITO. The Institute of Scientific and Industrial Research, Osaka University (8-1 Mihogaoka, Ibaraki 567-0047)

の進ちょくについては報告が少ない．

なお近年，中枢神経系に対する神経インターフェースについてもさまざまな成果が上がってきている．これは脳の各領域がある程度機能ごとに分かれているため，電極の実効集積度が低くとも末梢神経ほどは問題とならない点が大きい．実際，脳が体をどのように動かそうとしているかといった運動指示信号の抽出には，脳に設置した数十チャネル程度の電極が効果を発揮している[5,6]．しかしながら生体に感覚情報の入力を行うには，担当感覚器官に近い部位の末梢神経を対象にインターフェースを構築することが望ましい．

3. 要素技術1 ～高効率細胞膜せん孔デバイス～

90年代半ばに私が神経インターフェースの研究を開始した当初は，神経細胞に対して電極を使わず，光学的に情報入力を行えないかと考えていた．残念ながら当初の実験は失敗し，細胞に作用させた添加物ビスアミノメチルターチオフェン（BAT）[7]による影響で細胞を即死させてしまった．BATは天然の光毒素αターチエニル（α-T）[8]の水溶性誘導体であり，光照射により電荷が変化する性質がある．この分子が細胞をONにする電位感受性ナトリウムイオンチャネル（細胞膜にある一種のゲート素子）の近傍にあれば，光照射に伴う電位変化によりイオンチャネルを強制的に開放できると考えていた．そのもくろ見は外れたが，細胞死に至る過程を調べてみると，細胞膜抵抗が半減するほどの膜傷害が生じても，数十秒程度で抵抗が回復している状態があることがわかった[9]．そこでこれは細胞内電極のための，新たな細胞膜せん孔法につながると考え直したのである．

そして傷害機構は光酸化反応によるという傍証を固めたうえで[10]，この細胞膜せん孔を，細胞を対象に微小ガラス管で注射を行うマイクロインジェクション法に適用した結果，注入処理後3日目に約9割の生存率を達成した[11]．さらに理化学研究所との共同成果として，機能性色素，抗体，mRNAをラット神経系の細胞に注入し，細胞の生存および注入した物質の機能が発現することを確認した（図2(a)）[12]．

次の課題は集積型神経インターフェースの鍵として，安価かつ大規模に細胞膜せん孔法を実施することが可能かという点になった．光化学反応による細胞膜せん孔は，光増感剤・光触媒を細胞に局地的に接触させて光照射を行うだけであり，細胞に対する作業の精度が低くとも実施可能である．この点が既存の機械的・光学的なせん孔と異なり，本質的に大規模化に適したゆえんである．

例えば近年，集束イオンビームにより走査プローブ顕微鏡の探針を精密加工した細胞膜せん孔体が報告されている[13]．これは最大で400 nm径の精密丸棒であり，細胞死をほとんど誘発せず遺伝子導入を行える．一細胞対象であれば，細胞に対して毒である酸化反応を使用しない分，光化学細胞膜せん孔法よりも優れると考えられる．しかし生体内の神経細胞群を対象とするような数万～数百万単位でのせん孔体集積化を，ランニングコストの高価な集束イオンビームで行うのは費用面で困難と考えられる．

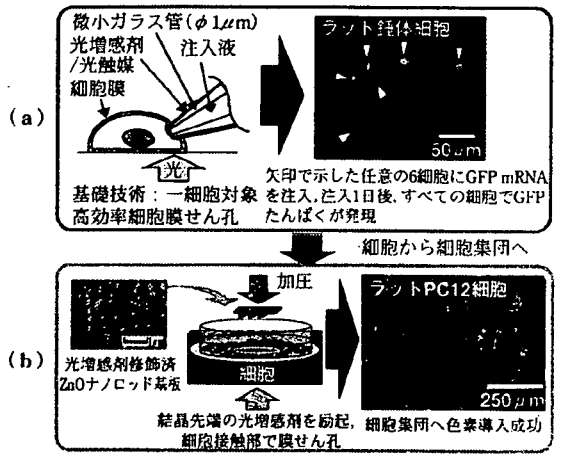

図2 高効率細胞膜せん孔法[12,14]．

以上のような細胞用途に適した，安価に大規模集積が可能な剣山状構造体を検討した結果，ナノロッド（Whisker，ひげ結晶とも呼称）を試みることとした．細胞実験用に用意した酸化亜鉛ナノロッドは，自己組織化によるVapor-Liquid-Solid（VLS）成長に基づき形成され，また結晶先端には金が高濃度で残存するため，それまで使用してきたBATやα-Tなどチオフェン系光増感剤の硫黄原子と自己組織的な結合が可能という特長がある．

現段階の成果として，上記の自己組織化ナノプロセスと細胞膜せん孔法の融合によって，細胞処理の規模拡大に十分な可能性を示す実験成果を得ている．せん孔には酸化亜鉛ナノロッド基板にα-Tを修飾したものを使用し，この基板によって70 g/cm^{2}程度の圧力で培養ディッシュ上のラットPC12細胞群を圧迫し，増感剤を励起する光照射を行った．その結果，従来の一細胞を対象とした光化学細胞膜せん孔と同様に，細胞外の水溶性蛍光マーカー分子が細胞内に取り込まれ，細胞集団を対象に細胞膜せん孔が達成された結果が得られている（図2(b)）[14]．この成果により，導入自由度の面で問題の多い既存の遺伝子導入法を上回る応用の見通しが立ち，企業との連携が具体化した．さらにこの膜せん孔技術の集積化パッチ電極アレイへの適用について立命館大学と共同研究を行っており，すでに成果が出始めている[15]．

今後，細胞レベル神経インターフェースとして細胞膜せん孔技術を育成するには，細胞内に電極を挿入し続けられるのか，素材面などで解決すべき課題はまだ多いと思われる．しかしながら，この技術の特長は，個々の細胞を一種の電気・化学的な情報処理素子として，直接にせん孔して自由度の高い機能改変を行いうる汎用性にある．このため将来的には電極側に限らず，細胞側にも神経インターフェースのための最適化処理を施せるよう，生化学的な用

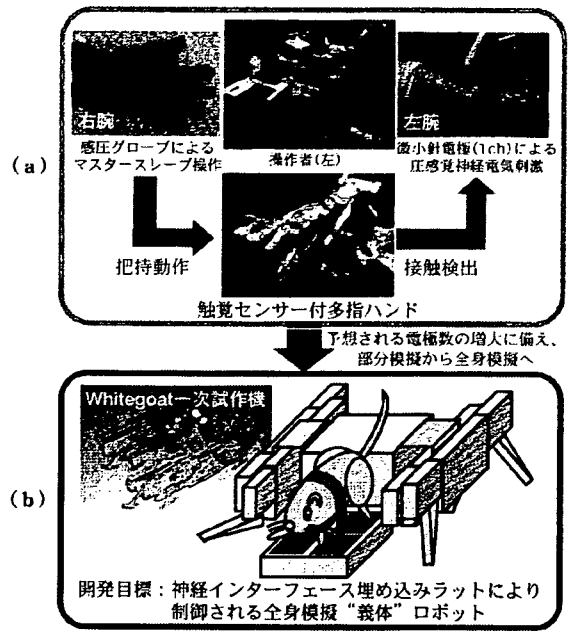

図3 神経インターフェースと連動する身体模擬ロボット[17,18].

途開拓にも努めたい.

4. 要素技術2 ～動物模擬ロボット～

神経インターフェースの開発においては，インターフェースを通じて生体-機器間でどのような情報が授受されているか確認する必要がある．既存の細胞外電極を使用した情報伝達については，われわれはすでにヒト末梢神経の一線維を対象とした電気刺激によって，定量的な圧力感覚の伝達に成功している[15]．これは神経制御義手のプロトタイプとして開発した，ロボットハンドに対する圧力をハンド操作者が神経刺激経由で実際に感じ，フィードバックをかけるシステムの中核である（図3(a)）[17]．このようにヒトが対象であれば，例えば神経インターフェースからの入力の結果，得られた感覚について質問し，その結果を反映して改良を行うことができる．しかし細胞レベル神経インターフェースといった新しいデバイスは，まず動物実験が必要になる．この場合，動物に質問を行うのは困難であるため，神経インターフェースが機能中の動物の反応を，外部から的確に確認することが重要となる．このため，動物の体に相当するロボットを用意し，動物とロボットの動きを比較することで，インターフェースの妥当性を検討する方法が多く用いられている[5,6]．

現在はインターフェースが媒介する情報量が乏しいため，腕のみ，あるいは脚のみといった，部分模擬ロボットが用いられているが，媒介情報量の大きい細胞レベル神経インターフェースの開発に備えて，全身を模擬した「義体」とでも呼べるロボットが必要になる（図3(b)，図4）．われわれの試作ロボット“Whitegoat”は，このような用途を追求して開発された[18]．すなわち脚で，動物の望む方向へ望む速度で，かつ動物本体や計測装置を搭載して移動できるという仕様である．なお機体名は，ヤギ用人工心臓の電装系を応用していることに由来する．

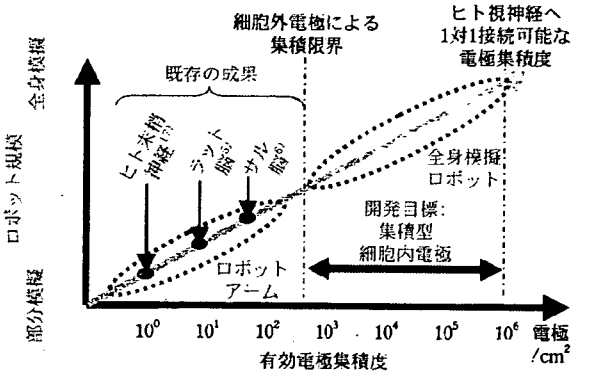

図4 神経電極集積度と評価用ロボットの規模.

この機体開発に際しては，かわさきロボット競技大会（主催：(財) 川崎市産業振興財団）が参考となっている．同大会は1994年より毎年開催され，参加機体には規定の連続回転型モーターを利用した，リンク機構による歩行が義務づけられている．競技内容は不整地での格闘戦ということもあり，強豪チームの機体はきわめて高い耐久性と移動・運搬性能を達成している．動物模擬ロボットの必要スペックを，個別の関節を分散動力で駆動する方式で達成するには非常な困難が続くと思われるが，かわさき大会では古典的なリンク機構を深めることで，それに近い水準に至っていた．

その影響もあり，“Whitegoat”においては，あえて集中動力源による古典的なリンク機構を主な脚駆動手段とし，脚の旋回機構を副次的に組み合わせることで，多彩な歩行を実現した．自重の保持と動力伝達を機構的に分けた，旋回可能な脚構造が独自技術であり，科学技術振興機構から特許出願がなされている[19]．

5. ロボット派生技術

派生技術も含めたロボットの現状を図5に示す．動物に近い移動・運搬性能を目指したわれわれの試作ロボットは，結果的に実用ロボットに求められる性能に近づくことになった．すなわち脚移動機構によるものでは世界最高レベルの運搬性能と運動性能を有し，加えて量産に適したシンプルな構造となっている．また過去には脚旋回構造こそ含まないものの，“Whitegoat”とほぼ共通の駆動系をもつ50 cc内燃機関を搭載した有人試作機（図5(a)）も存在したことから，本機には大型乗用ロボットとしての発展性もあると考えている．

昨年には新たな技術要素として，移動補助にも使用可能なマニピュレーター機構を開発（図5(b)），特許出願を行った．これは全長20 cm程度とコンパクトに収納可能，かつ5 m程度であれば直進性よく目指す場所まで伸ばせ，過負荷に対しては可逆的に屈曲可能な棒状構造体であ

図5　ロボット関連技術の発展性.

る[20].

マニピュレーター機構とロボットの組み合わせは，動物のような跳躍とは異なるが，自機の昇降，あるいは登はんにより，動物的な立体移動能力をもたせることができる．このマニピュレーターは人工衛星用アンテナ技術[21]を源流としたもので，産業界からもさまざまな用途への期待を集めている．

このような継続的なシーズ・ニーズ開拓により，本来の目的である神経インターフェース評価用も含めた量産ロボットの早期実現につなげたい．

6. むすび

細胞レベル神経インターフェースを志向して進めてきた研究は，神経に限らず個々の細胞を電気・化学的な情報処理素子として扱うという，より大きなコンセプトに結実しつつある．現在まで述べてきた内容は，あくまでも神経細胞を一種の配線として扱うものであるが，実際の神経細胞は演算素子でもある．その記憶・演算機能の人工物との複合化については，応用物理の研究者に新たに大きな活躍の場を提供すると考えられる．また動物模擬ロボットも，新規なデバイスや制御アルゴリズムの試験，あるいはデモンストレーションに使える汎用性がある．

この技術と組み合わせて画期的な新領域を切り開ける方には，ぜひお手伝いさせていただきたい．興味をもたれた方は私宛に遠慮なく問い合わせいただければ幸いである．

文　献

1) A.L. Hodgkin and A.F. Huxley : J. Physiol. **117** (4), 500(1952).
2) E. Neher and B. Sakmann : Nature **260**, 799(1976).
3) J.S. Titiyal, M. Ray, N. Sharma, R. Sinha and R.B. Vajpayee : Cornea **21** (6), 615(2002).
4) S. Kurata, M. Tsukakoshi, T. Kasuya and Y. Ikawa : Exp. Cell Res. **162**, 372(1986).
5) J.K. Chapin, K.A. Moxon, R.S. Markowitz and M.A.L. Nicolelis : Nature Neuroscience **2**, 664(1999).
6) J. Wessberg, C.R. Stambaugh, J.D. Kralik, P.D. Beck, M. Laubach, J.K. Chapin, J. Kim, S.J. Biggs, M.A. Srinivasan and M.A.L. Nicolelis : Nature **408**, 361(2000).
7) H. Muguruma, T. Saito, S. Sasaki, S. Hotta and I. Karube : J. Heterocyclic Chem. **33**, 1(1996).
8) J. Bakker, F.J. Gommers, I. Nieuwenhuis and H. Wynberg : J. Biol. Chem. **254**, 1841(1979).
9) T. Saito, N.A. Hartell, H. Muguruma, S. Hotta, S. Sasaki, M. Ito and I. Karube : Photochem. Photobiol. **68**, 745(1998).
10) T.K. Saito, M. Takahashi, H. Muguruma, E. Niki and K. Mabuchi : J. Photochem. Photobiol., B : Biol. **61**, 114(2001).
11) T.K. Saito, H. Muguruma and K. Mabuchi : Biotechnol. lett **24**, 309(2002).
12) R. Yano, D. Okada, C.C. Yap, K. Mabuchi, H. Muguruma and T.K. Saito : NeuroReport **13**, 1263(2002).
13) Obataya, I. Nakamura, C. Han, S. Nakamura and N. Miyake : J. Nano Lett. **5** (1), 27(2005).
14) 齋藤　敬, 関　宗俊, M.A. El-Maghraby, 大石聡司, 田畑　仁 : 第53回応用物理学関係連合講演会予稿集, 24p-I-8 (2006).
15) K. Iso, T.K. Saito, H. Muguruma, H. Tabata and S. Konishi : 20th IEEE Internat. Conf. on Micro Electro Mech. Sys. 445 (2007).
16) 鈴木隆文, 齋藤　敬, 國本雅也, 満渕邦彦 : 日本バーチャルリアリティ学会論文誌 **11**(1), 95(2006).
17) M. Shimojo, T. Suzuki, A. Namiki, T. Saito, M. Kunimoto, R. Makino, H. Ogawa, M. Ishikawa and K. Mabuchi : Proc. of 2003 IEEE Internat. Conf. on Robotics and Automation CD-ROM, 1264(2003).
18) T.K. Saito, I. Saito, N. Nemoto, K. Takiura, T. Ozeki, N. Kakuta, T. Tohyama, T. Isoyama and T. Chinzei : Springer Tracts in Advanced Robotics **24**, 385(2006).
19) 特開2003-266336「多脚歩行ロボット」齋藤　敬.
20) 特願2006-226099「マニピュレータ機構」齋藤　敬.
21) F.P.J. Rimrott : Machine Design **37** (28), 156 (1965).

(2007年8月2日　受理)

齋藤　敬（さいとう　たかし）

1999年東京大学先端学際工学博士課程修了．東京大学国際・産学共同研究センターリサーチアソシエイトなどを経て，05年大阪大学産業科学研究所特任助教授，07年同特任准教授，現在に至る．博士(工学)．任期なしでの雇用先募集中．

平成19年5月25日

各　　位

会 社 名　株式会社 アテクト
代表者名　代表取締役社長　小髙 得央
（ＪＡＳＤＡＱ・コード４２４１）
問い合わせ先
責任者役職名　管理ディヴィジョンリーダー
氏　　名　水馬　暁
ＴＥＬ（072）967 － 7000（代表）

遺伝子や薬剤を細胞に導入するための新規細胞膜穿孔技術の応用開発に関する産学共同研究に関するお知らせ

当社と国立大学法人大阪大学（本部：大阪府吹田市 総長：宮原秀夫）は、このたび、細胞内に遺伝子や薬剤を導入するための新規細胞膜穿孔技術の商品開発に関して、平成１９年４月１９日から平成２０年３月３１日までの予定（発展性に応じて延長）で共同研究を開始いたしましたので、下記のとおりお知らせいたします。

－ 記 －

本共同研究は、大阪大学産業科学研究所 齋藤 敬 特任准教授が発明者である「光酸化触媒による細胞膜穿孔技術」を利用したデバイスの有効性評価と応用例の拡充を目的としております。本共同研究の基盤となる技術は、高効率、高生存率で細胞に大量の遺伝子や薬剤を導入可能であることが一部の細胞に対して確認されており、今期は応用例と有効性の評価のデータをもとに、量産可能なキット化を目指した開発を実施し、細胞内へ遺伝子や薬剤を大量導入する新規技術を応用したデバイスの上市を目指します。

細胞内に遺伝子などを導入する主たる技術には、マイクロインジェクション法(※１)およびエレクトロポレーション法(※２）が挙げられます。前者は一つの細胞に多種類の遺伝子や巨大分子を導入することができる反面、処理後の生存率が低くなるという短所があります。一方、後者は大量の細胞を同時に高生存率で処理できる反面、穿孔径が小さく多種類の遺伝子や巨大分子を導入する効率が低いという短所があります。本共同研究の基盤となる技術は両者の短所を克服できるものです。

本デバイスは一定圧のもとで光を照射するというシンプルな細胞膜穿孔技術であり、複雑な条件検討や特殊技術を必要とせず、大量の細胞に遺伝子や生理活性物質などを効率的に導入できます。本デバイスが商品化されることにより、研究・開発用途としては、細胞機能の解析や生理活性物質の導入による細胞挙動解析が迅速に行えるようになるとともに、遺伝子導入による動植物細胞の改良や機能強化なども効率的に行うことが期待されます。また中長期的には、創薬スクリーニングや個々の人に合わせたテーラーメイド医療など、医薬分野に貢献する基盤デバイスとしても期待されます。

※1　マイクロインジェクション法：細胞に微小ガラス管を刺入して、遺伝子や物質を注射する技術。

※2　エレクトロポレーション法：電気穿孔法とも呼ばれる方法で、細胞膜にパルス的に高電圧をかけることにより生存に影響のないあるいは影響力の低い程度の穴を開け、その穴から目的物質を導入する技術。

以　　上

+Model
NSL-24423; No. of Pages 6

Available online at www.sciencedirect.com
ScienceDirect
Neuroscience Letters xxx (2007) xxx–xxx
Neuroscience Letters
www.elsevier.com/locate/neulet

Sema4D-plexin-B1 implicated in regulation of dendritic spine density through RhoA/ROCK pathway

Xianzong Lin[a,b], Mariko Ogiya[b], Mizue Takahara[b], Wataru Yamaguchi[b], Tatsuo Furuyama[b,c], Hidekazu Tanaka[d], Masaya Tohyama[a], Shinobu Inagaki[b,*]

[a] Department of Anatomy and Neuroscience, Osaka University Graduate School of Medicine, Yamadaoka 2-2, Suita, Osaka 565-0871, Japan
[b] Group of Neurobiology, Division of Health Sciences, Osaka University Graduate School of Medicine, Yamadaoka 1-7, Suita, Osaka 565-0871, Japan
[c] Department of Nutrition, School of Human Health, Sonoda Women's University, Amagasaki, Hyogo 661-8520, Japan
[d] Department of Pharmacology, Osaka University Graduate School of Medicine, Yamadaoka 2-2, Suita, Osaka 565-0871, Japan

Received 23 July 2007; received in revised form 2 September 2007; accepted 19 September 2007

Abstract

Plexin-B1, Sema4D receptor, mediates retraction and extension signals in axon guidance by associating with PDZ-containing Rho guanine nucleotide exchange factors (PDZ-RhoGEFs) which can activate a small Rho GTPase RhoA. RhoA is implicated in spine formation by rearranging actin cytoskeleton. Exogenous application of Sema4D to cultured neurons caused activation of RhoA, increase of spine density and changes in spine shape. Sema4D-induced changes in spine density were blocked by either Rho-kinase (a downstream of RhoA, ROCK) inhibitor Y-27632 or by overexpression of plexin-B1 mutant lacking the C-terminus which no longer associates with PDZ-RhoGEFs. This study suggests that Sema4D-plexin-B1 play a crucial role in spine formation by regulating RhoA/ROCK pathway.

Keywords: Semaphorin; Plexin; Rho; Dendritic spine; Cytoskeleton; Neuron

Semaphorins comprise a family of soluble and transmembrane proteins that play a critical role in axon guidance in the developing nervous system [16,18,32]. Semaphorins trigger dynamic rearrangements of actin cytoskeleton and induce retraction or extension of neurites [3,17,19,20,25,28]. Expressions of several semaphorins and their functional receptors, plexins, persist into adulthood after axon guidance has been completed [10,15,19–21,33,36]. However, roles of semaphorins at postnatal ages are not well understood.

Dendritic spines, actin-rich protrusions on neuronal dendrites, are the major postsynaptic sites of excitatory synapses in the brain [7,11–13]. The spine formation and morphology are regulated by reorganizing actin cytoskeleton [4,12]. Rho GTPases, RhoA, Rac and Cdc42 are important in this regulation [22,34]. They are active when bound to GTP and inactive when bound to GDP, act as intracellular molecular switches and transduce signals from extracellular stimuli to the actin cytoskeleton. However, little is known about external cues that trigger the activation of Rho GTPases in spine formation and morphogenesis. Sema4D is such a candidate, because it and its receptor plexin-B1 are highly expressed in the brain during early postnatal period the synaptic formation stage [9,36], and mediate RhoA-signaling via direct association with PDZ (postsynaptic density-95/Discs large/zona occludens-1) domain-containing Rho guanine nucleotide exchange factors (PDZ- RhoGEFs) (positive regulators of RhoA activation), p190-Rho guanine nucleotide activating protein (RhoGAP) (a negative regulator of RhoA-signaling), and a RhoGTPase Rnd1 [3,13,23,26,33]. Here, we investigate whether Sema4D-plexin-B1 is involved in spine formation and morphogenesis of cultured hippocampal neurons via RhoA/Rho-kinase (ROCK) pathway.

Hippocampal neurons were cultured as described by Banker and Goslin [2] with modifications. In brief, the hippocampal tissues were dissociated from Sprague-Dawley rat embryos of embryonic day 18 (E18) (SLC), and digested in 10 ml of 4 U/ml papain (Worthington Biochem)/0.0015% DNase (Sigma)/0.02 M phosphate buffered saline (PBS)/0.2 mg/ml DL-cysteine HCl/0.2 mg/ml bovine serum albumin (BSA) (Sigma)/5 mg/ml glucose in 50 ml tube for 15 min at 37 °C.

* Corresponding author. Tel.: +81 6 6879 2581; fax: +81 6 6879 2581/2629.
E-mail address: inagaki@sahs.med.osaka-u.ac.jp (S. Inagaki).

0304-3940/$ – see front matter © 2007 Elsevier Ireland Ltd. All rights reserved.
doi:10.1016/j.neulet.2007.09.045

Please cite this article in press as: X. Lin, et al., Sema4D-plexin-B1 implicated in regulation of dendritic spine density through RhoA/ROCK pathway, Neurosci. Lett. (2007), doi:10.1016/j.neulet.2007.09.045

Suspended neurons were plated at 150 cells/mm^2 onto coverslips (Matsunami Glass), which were coated overnight with 2 mg/ml poly-L-lysine (Sigma) in 0.15 M borate buffer (pH 8.4). Neurons were cultured in Neurobasal medium (GIBCO)/B27 (GIBCO) and 25 μM L-glutamine. Two days after plating, the medium was exchanged with fresh Neurobasal/B27 every 3 days, and after 7 day-in vitro (DIV) one half of the medium was exchanged. Hippocampal neurons were transfected at 5-DIV with green fluorescent protein (GFP, Clonetech) together with or without a deletion mutant of plexin-B1ΔC (plexin-B1 lacking C-terminal three amino acids) by the calcium phosphate method as described [2,13]. Neurons were usually analyzed at 21-DIV.

Human embryonic kidney (HEK293) cells were cultured with 10% fetal bovine serum (FBS, Race, Australia)/Dulbecco's modified Eagle's medium (DMEM), and transfected with HA-tagged-human plexin-B1 (KIAA0407) [13], human plexin-B2 (KIAA0315) [13], and mouse plexin-A1 [15], and the cells were subjected to Western blot analysis. Sema4D-Fc (Fc-tagged extracellular region of mouse Sema4D) was obtained as described previously [8,9], and used as soluble Sema4D.

Polyclonal antibodies to plexin-B1 were raised by immunizing rabbits with maltose binding protein (MBP)-fused-mouse plexin-B1 (amino acid, 1216–1521, NM_17725). The specificity of the antibodies was confirmed by Western blot analysis. Mouse monoclonal antibody to HA was obtained from Boehringer–Mannheim, antibody to postsynaptic density protein (PSD-95) from Upstate Biotechnology and antibody to RhoA from Santa Cruz [13,14,37]. For Western blot analysis, primary antibodies were used at a dilution of 1:2000 (anti-plexin-B1, RhoA) and 1:10,000 (anti-HA), and for immunocytochemistry, anti-PSD-95 and anti-plexin-B1 were used at 1:500.

For Western blot analysis, cells were lysed in ice-cold lysis buffer (20 mM Tris–HCl pH 7.5, 1 mM EDTA–Na, 150 mM NaCl, 1% TritionX-100, 1 mM phenyl-methylsulfonyl fluoride (PMSF)), left on ice for 30 min, and the supernatant was pro-

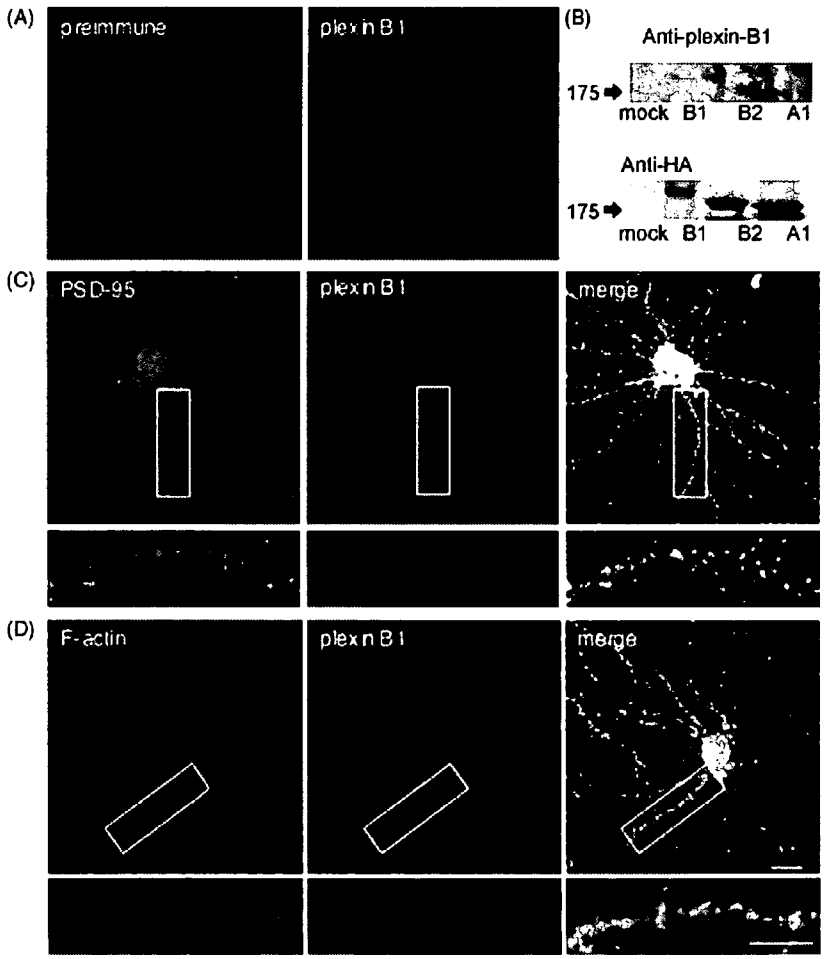

Fig. 1. Immunostaining for plexin-B1 in dendrites of cultured hippocampal neurons. (A) Cultured hippocampal neurons (21-DIV) were stained with the preimmune or the polyclonal antiserum to plexin-B1. (B) Western blot analysis shows the characteristics of the antiserum to plexin-B1. The antibodies recognize HA-tagged plexin-B1 (B1) but not plexin-B2 (B2) or plexin-A1 (A1) transfected in HEK 293 cells. (C and D) Immunofluorescent images of 21-DIV hippocampal neurons show localization of PSD-95 (green) and plexin-B1 (red) (C), and that of F-actin stained with FITC-phalloidin and plexin-B1 (red) (D). These images show colocalization of plexin-B1 with PSD-95 and with F-actin in dendritic spines. Scales: 10 μm (upper panels), 20 μm (lower panels). (For interpretation of the references to color in this figure legend, the reader is referred to the web version of the article.)

Please cite this article in press as: X. Lin, et al., Sema4D-plexin-B1 implicated in regulation of dendritic spine density through RhoA/ROCK pathway, Neurosci. Lett. (2007), doi:10.1016/j.neulet.2007.09.045

ceeded for SDS-PAGE electrophoresis and Western blot analysis as described previously [13]. The membrane was treated with 5% skim-milk/Tris–HCl (pH 7.5), incubated with primary antibody for 1 h, washed three times in 0.5% Tween 20/Tris–HCl, incubated with HRP-labeled secondary antibody (1:10,000) (Jackson Immunoresearch), and finally visualized by enhanced chemiluminescence ECL (Amersham).

Immunocytochemical staining was performed as described with modifications [14]. 21-DIV cultured hippocampal neurons and other cells were fixed in 10% formalin/PBS for 30 min, permeabilized with 0.25%Triton X-100/PBS for 10 min, washed in PBS twice, blocked in 10% BSA/PBS for 60 min, and then incubated with indicated primary antibodies in 3% BSA/PBS for 4 h at room temperature. After washed in PBS, cells were incubated for 2 h with Cy3- (1:2000) or FITC- (1:500) labeled goat anti-mouse or anti-rabbit-IgG (Jackson Immunoresearch), and/or FITC- (1:500) or TRIC-labeled phalloidin (1:1000) (Sigma). Neurons on coverslips washed in PBS were mounted in 95% glycerol on glass slides.

Serial confocal images of neurons were obtained with the LSM 510 confocal imaging system (Zeiss) using an oil immersion, 63× objective with sequential-acquisition as described previously [1,5,30]. Serial optical sections were taken at an interval of 0.5 μm for each image with 3× zoom. For measurement of spine density and morphology, spines located in the proximal 100-μm segments of the largest two dendrites were chosen from GFP-positive neurons, and manually traced. Then spine density and length were counted or measured automatically with LSM510 software (Zeiss). For each experimental group, more than 10 transfected neurons were chosen randomly for quantification from 3–4 coverslips derived from three independent experiments, and at least 200 spines were counted from more than 10 neurons visualized by GFP fluorescence as described elsewhere [5,30]. Spines were defined as described by Harris et al. [11]. Measured data were exported to Excel software (Microsoft), and the data were compared with Student's *t*-test. At least three independent experiments were performed for each experiment. Statistical significance was determined ($p < 0.01$) using Student's *t*-test.

Detection of active RhoA was performed as described previously [37]. Cultured neural cells (1×10^7 cells) prepared from cerebral cortex containing hippocampus were lysed in ice-cold lysis buffer (50 mM Tris–HCl, pH 7.5, 100 mM NaCl, 10 mM $MgCl_2$, 10% glycerol, 1% Triton X-100, 1 mM PMSF). The supernatant was incubated with 16 μg of GST-rhotekin Rho-binding domain [29]. The bound RhoA was eluted by boiling in sample buffer for SDS-PAGE and subjected to Western blot analysis with anti-RhoA antibody.

To verify the expression of plexin-B1 in dendrites, primary cultured hippocampal neurons were immunostained with anti-plexin-B1 antibodies. Plexin-B1 immunoreactivity was seen in the neuronal cell bodies, dendrites and dendritic spines, while no specific immunostaining was found in the control sections immunostained with the preimmune serum (Fig. 1A). Western blot analysis showed that the antibody reacts with plexin-B1 overexpressed in HEK293 cells, while does not with plexin-

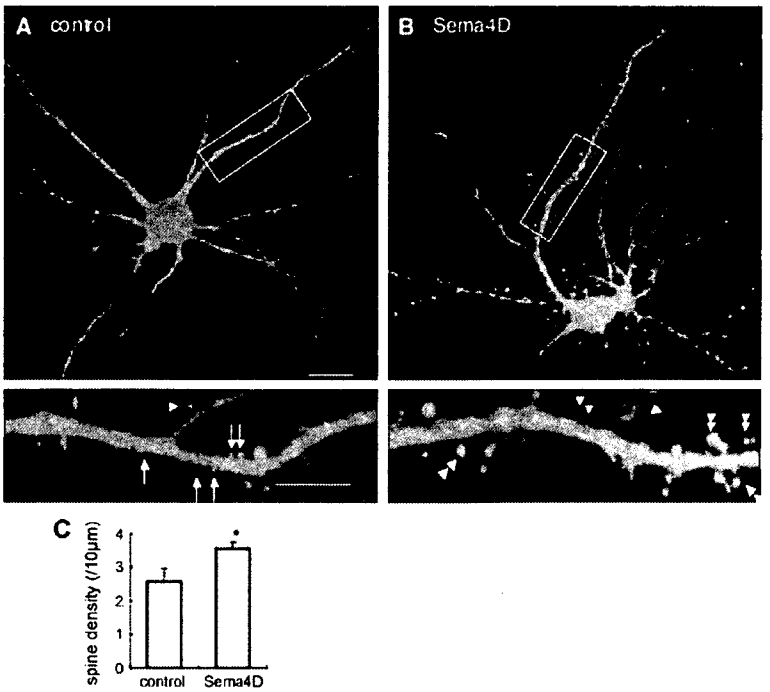

Fig. 2. Effects of Sema4D on dendritic spines. (A and B) Confocal GFP-images for dendritic morphology of cultured hippocampal neurons (21-DIV). Neurons transfected with GFP were untreated (A) or treated with 1 nM Sema4D-Fc for 6 h (B). Scales: 10 μm (upper panels), 20 μm (lower panels): Examples of stubby, thin and mushroom spines are indicated by arrows, arrowheads and double-arrowheads, respectively. (C) Spine density (per 10 μm-segment) was quantified in the proximal 100-μm-segments of the two largest dendrites from 15 neurons. Treatment of hippocampal neurons with Sema4D-Fc increased spine density. Data represent the mean spine density ± S.D. ($n = 15$ neurons per group), $^*p < 0.001$ with Student *t*-test.

Please cite this article in press as: X. Lin, et al., Sema4D-plexin-B1 implicated in regulation of dendritic spine density through RhoA/ROCK pathway, Neurosci. Lett. (2007), doi:10.1016/j.neulet.2007.09.045

B2 or plexin-A1 (Fig. 1B). Focusing on dendrites and dendritic spines, immunostaining for plexin-B1 was present in dendritic shafts and in punctuate structures along the shaft of hippocampal neurons. Dots-like plexin-B1-stainings were colocalized with PSD-95 (Fig. 1C), and also with F-actin (Fig. 1D). Our data show that plexin-B1 is endogenously expressed in dendritic spines and shafts.

In addition to the expression of plexin-B1 in dendrites, its ligand Sema4D is expressed in postnatal and adult brains [9,36]. To determine whether Sema4D-plexin-B1 contribute to spine formation we examined the effects of Sema4D on density of dendritic spines in cultured hippocampal neurons visualized by a transient transfection with GFP. Application of soluble Sema4D led to a significant increase of spine density (Fig. 2). The average density of dendritic spines was 2.58 ± 0.39 (per 10-μm) in control neurons treated with the control medium, while it was 3.56 ± 0.19 in neurons treated with the Sema4D-containing medium. Treatment with Sema4D had no significant affect on the length of spines (control, 0.93 ± 0.14 μm; Sema4D, 1.04 ± 0.09). Spine morphology is matured during development in the order of stubby, thin, and mushroom-types [6,11]. Stubby spines predominate in control 21-DIV hippocampal neurons, while thin and mushroom spines become predominant following treatment with Sema4D (Fig. 2). Taken together, our findings suggest that Sema4D promotes spine formation and morphological maturation of spines.

The effects of Sema4D on neurons are known to be mediated by plexin-B1 and its downstream signaling that is engaged in regulation of RhoA [13,26,33]. Sema4D-effect on RhoA was examined in whole cell lysates of neuron-rich culture from the cerebral cortex containing the hippocampus. Treatment with Sema4D induced activation of RhoA in cultured neurons (Fig. 3A). We therefore examined whether a major downstream effector of RhoA ROCK is involved in Sema4D-induced spine formation, using Y-27632, a specific ROCK inhibitor [35]. Treatment of hippocampal neurons with Y-27632 significantly reduced spine density (control, 2.48 ± 0.17/10 μm; Y27632, 1.72 ± 0.24) and eliminated Sema4D-induced increase in spine density (Sema4D, 3.57 ± 0.09/10 μm; Sema4D + Y-27632, 1.50 ± 0.16) (Fig. 3B and C). Simultaneous application of Y-27632 and Sema4D almost completely blocked Sema4D-induced increase in spine density. As previously described [27,34], Y-27632 increased the length of spines, while Y-27632 had no such effect when neurons were simultaneously treated with Sema4D (data not shown). These results suggest that RhoA/ROCK pathway is implicated in Sema4D-induced spine formation.

Sema4D can enhance active RhoA via plexin-B1 and its C-terminal association with PDZ-RhoGEFs [13,26,33]. To investigate whether the association of plexin-B1 with PDZ-RhoGEFs is required for Sema4D-induced changes in dendritic spines, plexin-B1ΔC mutant, which no longer associates with PDZ-RhoGEFs, was introduced into cultured hippocampal neurons. Transfection with plexin-B1ΔC completely blocked Sema4D-induced elevation of spine density (Fig. 4), while transfection with wild type-plexin-B1 did not block such Sema4D-induced elevation (data not shown).

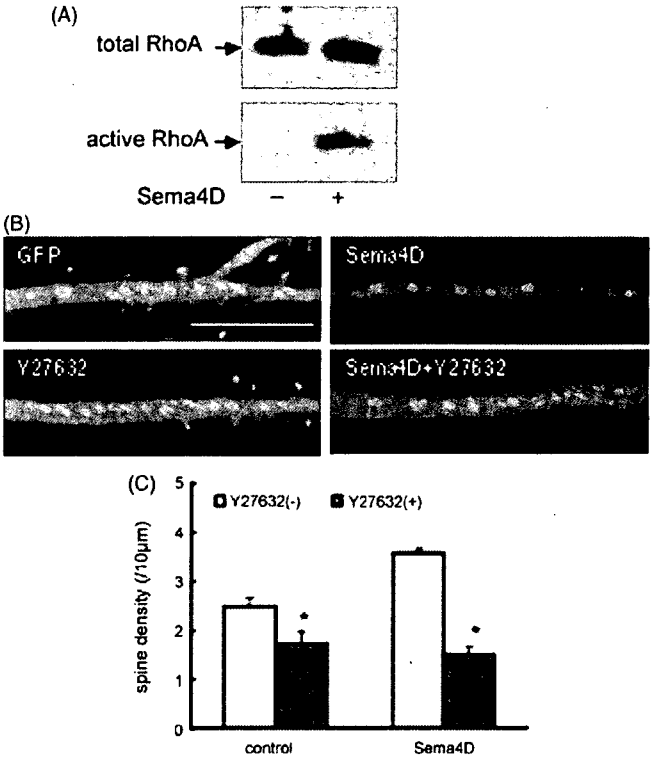

Fig. 3. Effects of Sema4D on neurons and blockade of ROCK. (A) Cultured cortical neurons (9-DIV) treated with or without 1 nM of Sema4D-Fc for 30 min. The lysates were incubated with GST-rhotekin beads. Bound active RhoA was subjected to SDS-PAGE followed by Western blot analysis with the anti-RhoA antibody. (B) Confocal GFP images show examples of dendritic spines of 21-DIV hippocampal neurons transfected with GFP. Neurons pretreated with or without 10 μM Y-27632, a ROCK inhibitor, were treated with or without 1 nM Sema4D-Fc for 6 h. Scale: 20 μm. (C) The effects of Y-27632 on spine density (per 10 μm-segment) were quantified from 15 neurons (two dendrites per neuron). Data represent the mean ± S.D. $*p < 0.001$ with Student t-test.

Plexin-B1 is widely found in the brain, and distributed in neuropils as well as over neuronal cell bodies in the hippocampus [33]. In this study, the immunostaining for plexin-B1 was confirmed in dendrites and dendritic spines, and it was colocalized with PSD-95, suggesting that plexin-B1can function as the receptor for Sema4D at dendrites and dendritic spines. The present data show that Sema4D plays a crucial role in regulating the spine density and morphology. Application of exogenous Sema4D increased the spine density, and thin and mushroom spines. Harris et al. [11] have shown that thin and mushroom spines containing postsynaptic density markedly increase in the hippocampus between postnatal day 15 and adult ages, correlating with synaptic strength. Changes in spine numbers and morphology are associated with neuronal development and changes in neuronal activity. The spine shape is important for its function as the postsynaptic component of excitatory synapses [38]. Increases in spine formation and maturation are most likely related to increases in excitatory synapse formation. Application of exogenous Sema4D increased active RhoA in the whole cell lysate of cultured neurons. Furthermore, Sema4D-induced increase in spine density was almost completely blocked by treatment of ROCK inhibitor Y-27632 and also by introduction

Please cite this article in press as: X. Lin, et al., Sema4D-plexin-B1 implicated in regulation of dendritic spine density through RhoA/ROCK pathway, Neurosci. Lett. (2007), doi:10.1016/j.neulet.2007.09.045

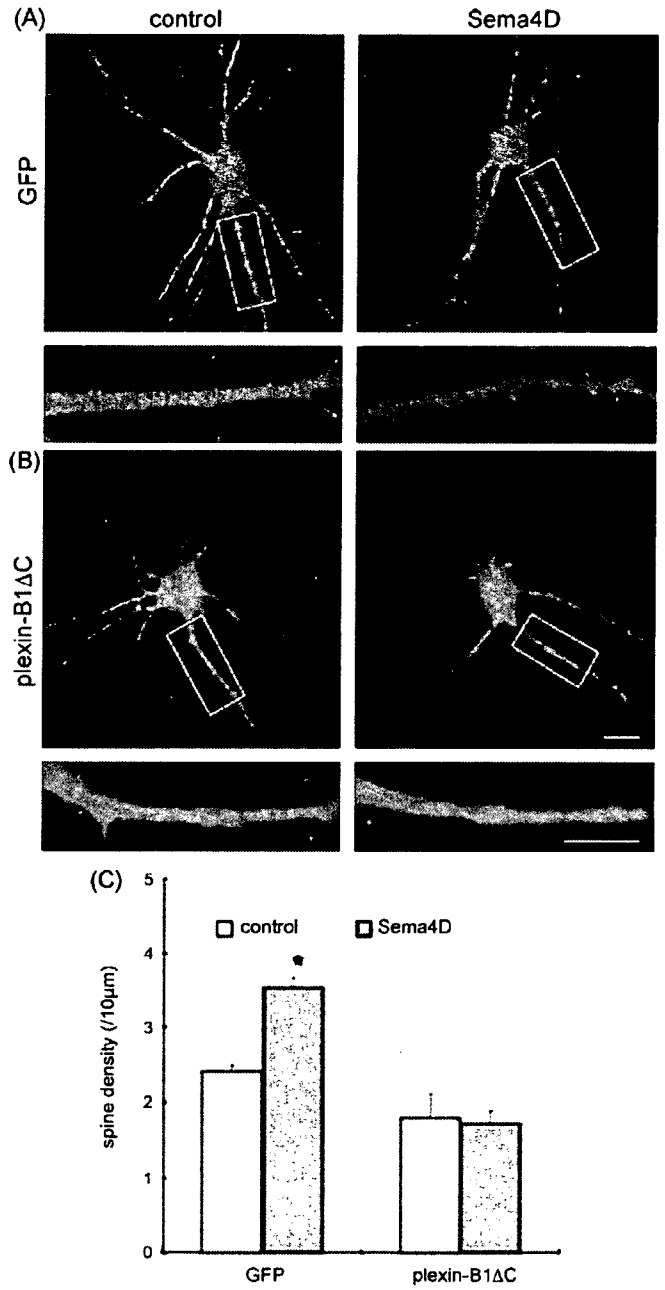

Fig. 4. C-terminus of plexin-B1 is required for the Sema4D effect on dendritic spines. (A and B) Confocal GFP-images were used to visualize dendritic morphology of cultured hippocampal neurons (21-DIV) transfected with GFP alone (A) and GFP with plexin-B1ΔC (B). Neurons were untreated (control) or treated with 1 nM Sema4D-Fc for 6 h. Scales: 10 μm (upper panels), 20 μm (lower panels). (C) Spine density (per 10 μm-segment) was quantified from 15 neurons as described above. $*p < 0.001$ with Student *t*-text.

of plexin-B1ΔC mutant. These findings suggest that Sema4D-plexin-B1 regulate spine density and probably spine morphology through the association with PDZ-RhoGEFs and its downstream RhoA/ROCK pathway.

Rho GTPases play an important role in dendritic spine formation [38]. Overexpression of constitutively active RhoA in the hippocampal slices promotes spine elimination and reduced spine density, while dominant negative RhoA does not affect spine density [4,34] Whereas, either inhibition of RhoA using C3 exoenzyme or blockade of ROCK using Y-27632 reduces spine density and increases the length of spines [27,34]. In coincidence with these reports, ROCK inhibitor Y-27632 reduced spine density and increased the length of spines in this study. Either active form of RhoA or inhibitor of RhoA signaling reduces spine density, suggesting that the balance between active and inactive forms of RhoA is important in spine formation. Besides PDZ-RhoGEFs, Sema4D can induce activation of p190RhoGAP, a ubiquitous GAP in the brain, which leads to a decrease of active RhoA [3]. The negative RhoA regulator p190RhoGAP also plays an important role in the functional activities induced by Sema4D-plexin-B1 such as cell collapse, inhibition of integrin-based adhesion, and neurite outgrowth [3]. Thus, it is possible that the complex interactions among PDZ-RhoGEF, p190RhoGAP and plexin-B1 exquisitely control RhoA [3,21,23,33].

A recent study by Schubert et al. [31] have shown that high potassium-induced reduction of spine density is accompanied by a decrease of active RhoA in the synaptosomes but an increase in the whole cell lysates, suggesting that the local RhoA at the synapses is implicated in regulation of spine density. It remains to be examined how RhoA become active at the spines or is localized to the spines in a time-dependent manner after addition of Sema4D. Recently, by using RNAi knockdown, Paradis et al. [24] have shown that reduction of endogenous expression of Sema4D had no effect on glutamatergic synapses but decreased GABAergic synapse density. In this study, Sema4D at higher level than endogenous one resulted in an increase of spine density. Taken together, Sema4D might differently regulate the density of excitatory or inhibitory synapses in a concentration-dependent manner. It is intriguing to investigate whether excitatory glutamatergic synapses increase in number at higher Sema4D level after the addition of it.

Acknowledgements

We are grateful to Dr. T. Nagase (Kazusa DNA Research Institute) for plasmids of KIAA0407 and KIAA0315, Dr. F. Suto (Nippon National Institute Genetics) for plexin-A1 and Dr. M. Uehata (Yoshitomi Pharmaceutical) for Y-27632. This study was supported in part by Grants-in aid for scientific research from the Ministry of Education, Science, Technology, Sports and Culture of Japan (SI).

References

[1] K. Abe, O. Chisaka, F. Van Roy, M. Takeichi, Stability of dendritic spines and synaptic contacts is controlled by alpha N-catenin, Nat. Neurosci. 7 (2004) 357–363.
[2] G. Banker, K. Goslin, Culturing Nerve cell, MIT Press, London, 1993.
[3] D. Barberis, A. Casazza, R. Sordella, S. Corso, S. Artigiani, J. Settleman, P.M. Comoglio, L. Tamagnone, p190 Rho-GTPase activating protein associates with plexins and it is required for semaphorin signaling, J. Cell Sci. 11 (2005) 4689–4700.
[4] I.M. Ethell, E.B. Pasquale, Molecular mechanisms of dendritic spine development and remodeling, Prog. Neurobiol. 75 (2005) 161–205.

Please cite this article in press as: X. Lin, et al., Sema4D-plexin-B1 implicated in regulation of dendritic spine density through RhoA/ROCK pathway, Neurosci. Lett. (2007), doi:10.1016/j.neulet.2007.09.045

[5] I.M. Ethell, Y. Yamaguchi, Cell surface heparan sulfate proteoglycan syndecan-2 induces the maturation of dendritic spines in rat hippocampal neurons, J. Cell Biol. 144 (1999) 575–586.
[6] J.C. Fiala, M. Feinberg, V. Popov, K.M. Harris, Synaptogenesis via dendritic filopodia in developing hippocampal area CA1, J. Neurosci. 18 (1998) 8900–8911.
[7] M. Fischer, S. Kaech, D. Knutti, A. Matus, Rapid actin-based plasticity in dendritic spines, Neuron 20 (1998) 847–854.
[8] S. Fujioka, K. Masuda, M. Toguchi, Y. Ohoka, T. Sakai, T. Furuyama, S. Inagaki, Neurotrophic effect of semaphorin 4D in PC12 cells, Biochem. Biophys. Res. Commun. 301 (2003) 304–310.
[9] T. Furuyama, S. Inagaki, A. Kosugi, S. Noda, S. Saitoh, M. Ogata, Y. Iwahashi, N. Miyazaki, T. Hamaoka, M. Tohyama, Identification of a novel transmembrane semaphorin expressed on lymphocytes, J. Biol. Chem. 271 (1996) 33376–33381.
[10] R.J. Giger, R.J. Pasterkamp, S. Heijnen, A.J. Holtmaat, J. Verhaagen, Anatomical distribution of the chemorepellent semaphorin III/collapsin-1 in the adult rat and human brain: predominant expression in structures of the olfactory-hippocampal pathway and the motor system, J. Neurosci. Res. 52 (1998) 27–42.
[11] K.M. Harris, F.E. Jensen, B. Tsao, Three-dimensional structure of dendritic spines and synapses in rat hippocampus (CA1) at postnatal day 15 and adult ages: implications for the maturation of synaptic physiology and long-term potentiation, J. Neurosci. 12 (1992) 2685–2705.
[12] H. Hering, M. Sheng, Dendritic spines: structure, dynamics and regulation, Nat. Rev. Neurosci. 2 (2001) 880–888.
[13] M. Hirotani, Y. Ohoka, T. Yamamoto, H. Nirasawa, T. Furuyama, M. Kogo, T. Matsuya, S. Inagaki, Interaction of plexin-B1 with PDZ domain-containing Rho guanine nucleotide exchange factors, Biochem. Biophys. Res. Commun. 297 (2002) 32–37.
[14] S. Inagaki, Y. Ohoka, H. Sugimoto, S. Fujioka, M. Amasaki, H. Kurinami, N. Miyazaki, T. Furuyama, Sema4C, a transmembrane semaphorin, interacts with a post synaptic density protein, PSD-95, J. Biol. Chem. 276 (2001) 9174–9181.
[15] T. Kameyama, Y. Murakami, F. Suto, A. Kawakami, S. Takagi, T. Hirata, H. Fujisawa, Identification of plexin family molecules in mice, Biochem. Biophys. Res. Commun. 226 (1996) 396–402.
[16] A.L. Kolodkin, D.J. Matthes, C.S. Goodman, The semaphorin genes encode a family of transmembrane and secreted growth cone guidance molecules, Cell 75 (1993) 1389–1399.
[17] B.P. Liu, S.M. Strittmatter, Semaphorin-mediated axonal guidance via Rho-related G proteins, Curr. Opin. Cell Biol. 13 (2001) 619–626.
[18] Y. Luo, D. Raible, J.A. Raper, Collapsin, a protein in brain that induces the collapse and paralysis of neuronal growth cones, Cell 75 (1993) 217–227.
[19] K. Masuda, T. Furuyama, M. Takahara, S. Fujioka, H. Kurinami, S. Inagaki, Sema4D stimulates axonal outgrowth of embryonic DRG sensory neurons, Genes Cells 9 (2004) 821–829.
[20] N. Miyazaki, T. Furuyama, T. Sakai, S. Fujioka, Y. Ohoka, N. Takeda, S. Inagaki, Developmental localization of semaphorin H messenger RNA acting as a collapsing factor on sensory axons in the mouse brain, Neuroscience 93 (1999) 401–408.
[21] C. Moreau-Fauvarque, A. Kumanogoh, E. Camand, C. Jaillard, G. Barbin, I. Boquet, C. Love, E.Y. Jones, H. Kikutani, C. Lubetzki, I. Dusart, A. Chedotal, The transmembrane semaphorin Sema4D/CD100, an inhibitor of axonal growth, is expressed on oligodendrocytes and upregulated after CNS lesion, J. Neurosci. 23 (2003) 9229–9239.
[22] A.Y. Nakayama, M.B. Harms, L. Luo, Small GTPases Rac and Rho in the maintenance of dendritic spines and branches in hippocampal pyramidal neurons, J. Neurosci. 20 (2000) 5329–5338.
[23] I. Oinuma, H. Katoh, A. Harada, M. Negishi, Direct interaction of Rnd1 with Plexin-B1 regulates PDZ-RhoGEF-mediated Rho activation by Plexin-B1 and induces cell contraction in COS-7 cells, J. Biol. Chem. 278 (2003) 25671–25677.
[24] S. Paradis, D.B. Harrar, Y. Lin, A.C. Koon, J.L. Hauser, E.C. Griffith, L. Zhu, L.F. Brass, C. Chen, M.E. Greenberg, An RNAi-based approach identifies molecules required for glutamatergic and GABAergic synapse development, Neuron 53 (2007) 217–232.
[25] R.J. Pasterkamp, J.J. Peschon, M.K. Springgs, A.L. Kolodkin, Semaphorin7A promotes axon outgrowth through integrins and MAPKs, Nature 424 (2003) 398–405.
[26] V. Perrot, J. Vazquez-Prado, J.S. Gutkind, Plexin B regulates Rho through the guanine nucleotide exchange factors leukemia-associated Rho GEF (LARG) and PDZ-RhoGEF, J. Biol. Chem. 277 (2002) 43115–43120.
[27] Y. Pilpel, M. Segal, Activation of PKC induces rapid morphological plasticity in dendrites of hippocampal neurons via Rac and Rho-dependent mechanisms, Eur. J. Neurosci. 19 (2004) 3151–3164.
[28] F. Polleux, T. Morrow, A. Ghosh, Semaphorin 3A is a chemoattractant for cortical apical dendrites, Nature 404 (2000) 567–573.
[29] X.D. Ren, M.A. Schwartz, Determination of GTP loading on Rho, Methods Enzymol. 325 (2000) 264–272, C.
[30] C. Sala, K. Futai, K. Yamamoto, P.F. Worley, Y. Hayashi, M. Sheng, Inhibition of dendritic spine morphogenesis and synaptic transmission by activity-inducible protein Homer1a, J. Neurosci. 23 (2003) 6327–6337.
[31] V. Schubert, J.S. Da Silva, C.G. Dotti, Localized recruitment and activation of RhoA underlies dendritic spine morphology in a glutamate receptor-dependent manner, J. Cell Biol. 172 (2006) 453–467.
[32] Semaphorin Nomenclature Committee, Unified nomenclature for the semaphorins/collapsins, Cell 97 (1999) 551–552.
[33] J.M. Swiercz, R. Kuner, J. Behrens, S. Offermanns, Plexin-B1 directly interacts with PDZ-RhoGEF/LARG to regulate RhoA and growth cone morphology, Neuron 35 (2002) 51–63.
[34] A. Tashiro, A. Minden, R. Yuste, Regulation of dendritic spine morphology by the rho family of small GTPases: antagonistic roles of Rac and Rho, Cereb. Cortex 10 (2000) 927–938.
[35] M. Uehata, T. Ishizaki, H. Satoh, T. Ono, T. Kawahara, T. Morishita, H. Tamakawa, K. Yamagami, J. Inui, M. Maekawa, S. Narumiya, 7 Calcium sensitization of smooth muscle mediated by a Rho-associated protein kinase hypertension, Nature 389 (1997) 990–994.
[36] T. Worzfeld, A.W. Puschel, S. Offermanns, R. Kuner, Plexin-B family members demonstrate non-redundant expression patterns in the developing mouse nervous system: an anatomical basis for morphogenetic effects of Sema4D during development, Eur. J. Neurosci. 19 (2004) 2622–2632.
[37] T. Yamada, Y. Ohoka, M. Kogo, S. Inagaki, Physical and functional interactions of the lysophosphatidic acid receptors with PDZ domain-containing Rho guanine nucleotide exchange factors (RhoGEFs), J. Biol. Chem. 280 (2005) 19358–19363.
[38] R. Yuste, T. Bonhoeffer, Morphological changes in dendritic spines associated with long-term synaptic plasticity, Ann. Rev. Neurosci. 24 (2001) 1071–1089.

Please cite this article in press as: X. Lin, et al., Sema4D-plexin-B1 implicated in regulation of dendritic spine density through RhoA/ROCK pathway, Neurosci. Lett. (2007), doi:10.1016/j.neulet.2007.09.045

Cell PRESS

Neuron

Activity-Induced Protocadherin Arcadlin Regulates Dendritic Spine Number by Triggering N-Cadherin Endocytosis via TAO2β and p38 MAP Kinases

Shin Yasuda,[1,6] Hidekazu Tanaka,[2,6,*] Hiroko Sugiura,[1,6] Ko Okamura,[2] Taiki Sakaguchi,[2] Uyen Tran,[4] Takako Takemiya,[1] Akira Mizoguchi,[3] Yoshiki Yagita,[5] Takeshi Sakurai,[5] E.M. De Robertis,[4] and Kanato Yamagata[1,*]

[1]Department of Neuropharmacology, Tokyo Metropolitan Institute for Neuroscience, Fuchu, Tokyo 183-8526, Japan
[2]Department of Pharmacology, Osaka University Medical School, Suita, Osaka 565-0871, Japan
[3]Department of Anatomy, Mie University School of Medicine, Tsu, Mie 514-8507, Japan
[4]Howard Hughes Medical Institute and Department of Biological Chemistry, University of California, Los Angeles, Los Angeles, CA 90095-1662, USA
[5]Department of Neuroscience, Mount Sinai School of Medicine, New York, NY 10128, USA
[6]These authors contributed equally to this work.
*Correspondence: htanaka@pharma1.med.osaka-u.ac.jp (H.T.), kyamagat@tmin.ac.jp (K.Y.)
DOI 10.1016/j.neuron.2007.08.020

SUMMARY

Synaptic activity induces changes in the number of dendritic spines. Here, we report a pathway of regulated endocytosis triggered by arcadlin, a protocadherin induced by electroconvulsive and other excitatory stimuli in hippocampal neurons. The homophilic binding of extracellular arcadlin domains activates TAO2β, a splice variant of the thousand and one amino acid protein kinase 2, cloned here by virtue of its binding to the arcadlin intracellular domain. TAO2β is a MAPKKK that activates the MEK3 MAPKK, which phosphorylates the p38 MAPK. Activation of p38 feeds-back on TAO2β, phosphorylating a key serine required for triggering endocytosis of N-cadherin at the synapse. Arcadlin knockout increases the number of dendritic spines, and the phenotype is rescued by siRNA knockdown of N-cadherin. This pathway of regulated endocytosis of N-cadherin via protocadherin/TAO2β/MEK3/p38 provides a molecular mechanism for transducing neuronal activity into changes in synaptic morphologies.

INTRODUCTION

Various cellular events have been correlated with synaptic plasticity, a mechanism that is believed to underlie learning and memory. Cell-adhesion molecules are among the proteins responsible for these cellular events (Bailey et al., 1992; Manabe et al., 2000; Sytnyk et al., 2006). Among them, N-cadherin, a classical cadherin cell-adhesion molecule abundantly expressed in hippocampal excitatory synaptic junctions, has been most intensely correlated with synaptic plasticity (Bozdagi et al., 2000; Murase et al., 2002; Okamura et al., 2004; Tanaka et al., 2000; Tang et al., 1998). In a previous study, we found that an activity-regulated synaptic cell-adhesion molecule, arcadlin, is also essential for synaptic plasticity (Yamagata et al., 1999). Arcadlin, the rat ortholog of human protocadherin-8 (pcdh8) and of mouse, *Xenopus*, and zebrafish paraxial protocadherin (PAPC), is a unique member of the protocadherin superfamily and has a distinct cytoplasmic region (Strehl et al., 1998; Yamagata et al., 1999; Yamamoto et al., 2000). In *Xenopus* and zebrafish, arcadlin/PAPC plays an important role in homophilic cell adhesion and gastrulation movements of the paraxial mesoderm (Kim et al., 1998; Yamamoto et al., 2000). Recently, *Xenopus* arcadlin/PAPC has been shown to downregulate the adhesion activity of C-cadherin, a classical cadherin of developing *Xenopus* (Chen and Gumbiner, 2006). The interacting partners of arcadlin/PAPC in the CNS have not been identified.

The activity of cell-adhesion molecules in synaptic membranes is regulated in part by endocytosis. ApCAM, an *Aplysia* neural cell-adhesion molecule, for example, becomes internalized in presynaptic membrane upon the acquisition of long-term potentiation (LTP) (Bailey et al., 1992). Clathrin-coated pits and vesicles have been found in postsynaptic dendritic spines (Cooney et al., 2002; Racz et al., 2004). One of the mechanisms that regulate the endocytosis involves p38 MAPK (Johnson and Lapadat, 2002; Zhu et al., 2002), a serine/threonine kinase that responds to various stress-related stimuli (Tibbles and Woodgett, 1999). TAO2, a MAP kinase kinase kinase (MAPKKK) initially isolated as a mammalian homolog of Ste20p in *S. cerevisiae* (Chen et al., 1999), serves as a regulator of the p38 MAPK. Extracellular stimuli, such as those of certain G protein-coupled receptors or insulin receptor, are transduced via TAO kinases to p38 MAPK in nonneural tissues (Chen et al., 2003). The p38 MAPK is highly expressed in the brain, where it is thought to be involved in synaptic plasticity (Thomas and Huganir, 2004). The functions of TAO kinases and their upstream receptors in the CNS are not known.

In this study, we have found that N-cadherin, the most abundant classical cadherin in hippocampal excitatory synapses (Benson and Tanaka, 1998), serves as a target of arcadlin/PAPC in the mammalian nervous system. Arcadlin is induced by neural stimulation and transported to the synaptic membrane, where it binds to and internalizes N-cadherin. During our investigations into the mechanism of this internalization, we cloned a spliced form of TAO2 kinase (TAO2β) that binds to the arcadlin intracellular domain. Homophilic interactions of arcadlin on the cell surface activate p38 MAPK through the activation of TAO2β. In turn, active p38 MAPK feeds-back on TAO2β, phosphorylating its carboxy-terminal domain at a specific serine. This triggers the coendocytosis of an N-cadherin-arcadlin complex. Furthermore, knockout of *arcadlin* in the mouse leads to an increase in dendritic spines in cultured neurons, and siRNA knockdown of N-cadherin recovered the spine density. We propose that endocytosis regulated by this signal transduction pathway involving a protocadherin, a MAPKKK that binds to its intracellular domain, a MAPK, and a classical cadherin regulates the adhesiveness of synaptic membranes and hence the number of spines in an activity-dependent way.

RESULTS

Arcadlin Interacts with N-Cadherin

Arcadlin is an activity-regulated cell-adhesion molecule whose expression level is very low in the resting brain but is vigorously induced by neural stimulation and recruited to the dendritic spine (Yamagata et al., 1999). Upon neural stimulation, such as maximal electroconvulsive seizure (MECS), arcadlin immunoreactivity increased and displayed a punctate distribution in the stratum lucidum of the hippocampal CA3 region, in which N-cadherin is also found (Figures 1A and 1B; Fannon and Colman, 1996).

In cultured hippocampal neurons, spontaneous synaptic activity causes detectable expression of arcadlin, which was increased by brief treatment with glutamate or elevation in cAMP with isobutyl methylxanthine (IBMX) and forskolin (Figures 1C and 1D and data not shown). Although N-cadherin is also known to be induced by elevating cAMP level in acute hippocampal slices (Bozdagi et al., 2000), there was no significant induction of N-cadherin in our culture (Figures 1C and 1D). This discrepancy is presumably due to the lack of glial support and the higher spontaneous activity of neurons in dispersed culture. The expression of arcadlin in cultures treated with IBMX and forskolin was confined to glutamate decarboxylase 65 (GAD6)-negative, non-GABAergic neurons (Figure 1E, arrow). In such neurons, arcadlin showed punctate distribution in dendrites (Figure 1F, arrow). The arcadlin puncta were not colocalized or apposed to the GAD6-puncta, which correspond to inhibitory axonal termini (Figure 1F, arrowhead). In contrast, the arcadlin-puncta colocalized with postsynaptic markers for excitatory synapses, such as PSD-95 and the NMDA receptor subunit NR1, as well as N-cadherin (Figure 1G). Arcadlin was expressed in developing axonal growth cones of young neurons, showing that arcadlin is also present in developing presynaptic membranes (Figure 1H, arrow).

We discovered the association of arcadlin with N-cadherin fortuitously during the course of immunoprecipitation studies of N-cadherin in hippocampal lysates. Arcadlin was coimmunoprecipitated with N-cadherin in dissected rat hippocampi 4 hr after electroconvulsions, but very little was found in unstimulated hippocampi (Figure 1I; note that the amount of β-catenin bound to N-cadherin is not affected). Coimmunoprecipitation was detectable in resting cultured neurons, which was increased by neural stimulation, such as depolarization by KCl (Figure 1J). Another synaptic classical cadherin, cadherin-11, was also found to be associated with the induced arcadlin in the brain (Figure 1K). The fact that arcadlin is targeted to multiple classical cadherins is reminiscent of the notion that *Xenopus* arcadlin/PAPC downregulates the adhesion activity of C-cadherin (Chen and Gumbiner, 2006). In this study, we focused on N-cadherin as the most abundant example of these cadherins. Coimmnoprecipitation experiments from cocultured cell lines transfected with *N-cadherin* and *arcadlin* independently (single transfections) or simultaneously (cotransfection) revealed that they associated laterally in the same membrane (Figure 1L). Consistently, we were able to localize their interaction domains to their transmembrane segments by deletion mutant analyses (Figures 1M and 1N). The affinity of N-cadherin to arcadlin was significantly reduced by a point mutation L561P or L561P/M562G in the middle of the transmembrane α-helix of N-cadherin (Figures 1M and 1O). The corresponding amino acid of E-cadherin plays a pivotal role in homophilic *cis* dimerization (Huber et al., 1999).

Arcadlin Induces the Internalization of N-Cadherin

To test whether arcadlin had any effect on the adhesive activity of N-cadherin, we performed cell-aggregation assays using L929 cells (Takeichi, 1977). Although arcadlin itself has a homophilic adhesive activity, it is too weak to be detected in the aggregation assay optimized for classical cadherins (Yamagata et al., 1999). We found that arcadlin downregulated the homophilic adhesiveness of N-cadherin (Figures 2A and 2B). The inhibitory effect was not attributable to either the expression level of N-cadherin (Figure 2C) or the intracellular molecules associated with N-cadherin, such as catenins (Figure 2D). We therefore hypothesized that the downregulation of N-cadherin activity could involve the internalization of N-cadherin by analogy to the case of apCAM (Bailey et al., 1992) and L1 (Kamiguchi and Lemmon, 2000). Recently, a key role for endocytosis in the disassembly of E-cadherin cell-cell adhesion has been reported (Troyanovsky et al., 2006).

To examine whether arcadlin enhances the internalization of N-cadherin, we first quantified surface N-cadherin level by labeling neuronal proteins on the extracellular surface with biotin. The biotin-labeled surface proteins were

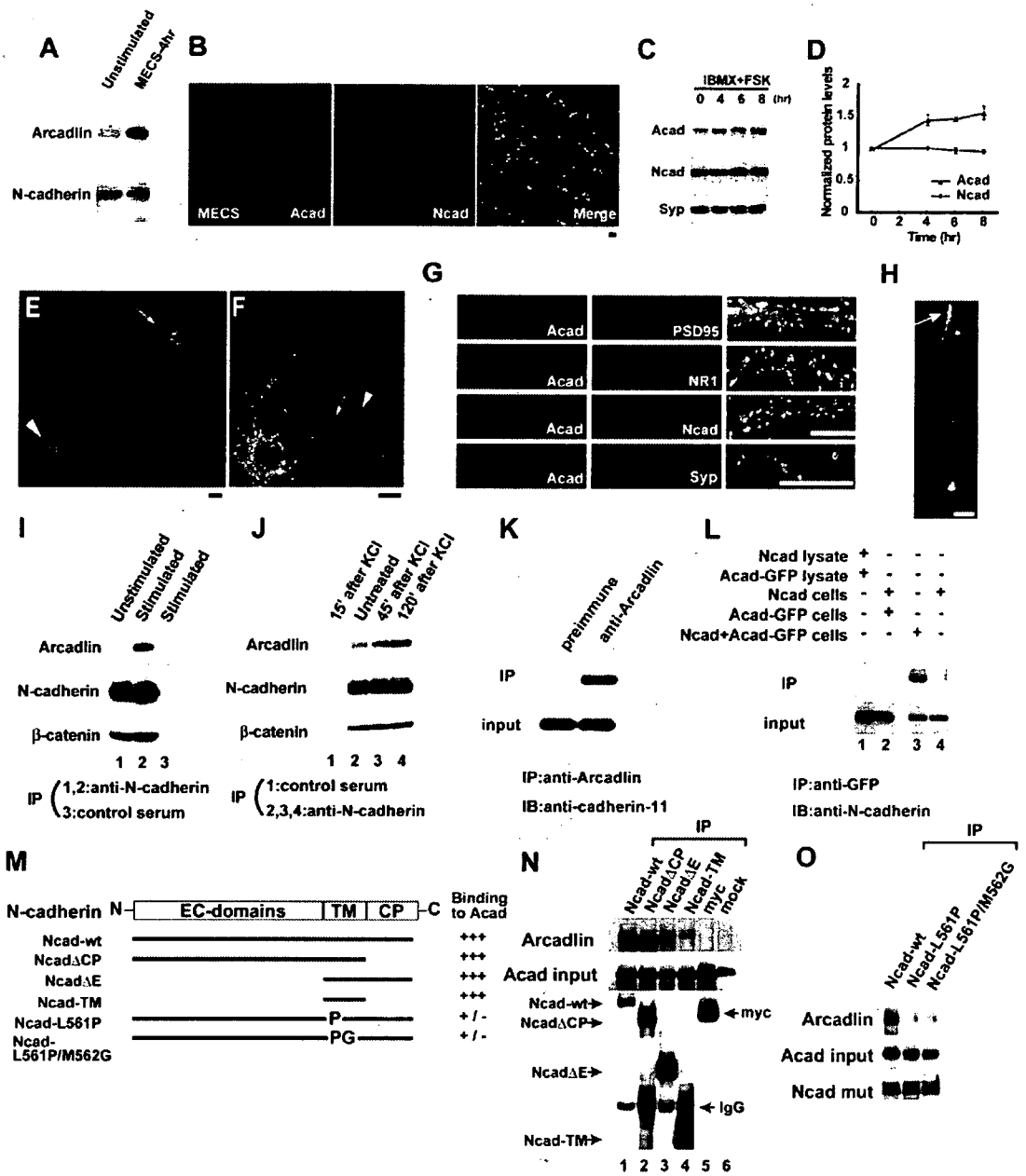

Figure 1. Arcadlin Is Associated with N-Cadherin at Hippocampal Synaptic Puncta

(A) Hippocampal extracts from unstimulated (control) and electroconvulsive shocked (MECS-4hr) rats were immunoblotted for arcadlin and N-cadherin.

(B) CA3 stratum lucidum doubly immunolabeled for arcadlin (Acad, green) and N-cadherin (Ncad, red) 4 hr after MECS. Significant colocalization confirmed ($r = 0.51$).

(C) Elevation of cAMP by IBMX and forskolin (FSK) induces the expression of arcadlin in cultured hippocampal neurons as examined by immunoblots. Syp, synaptophysin.

(D) The graph shows the relative band intensities of arcadlin and N-cadherin normalized with the bands for synaptophysin (mean ± SEM).

(E) Hippocampal neurons treated with IBMX and forskolin for 4 hr and immunostained for arcadlin (green) and GAD6 (red).

(F) An excitatory neuron double labeled for arcadlin (green) and GAD6 (red).

(G) Neurons double labeled for arcadlin (green) and PSD-95 (red; $r = 0.43$), NR1 (red), N-cadherin (red; $r = 0.36$), or synaptophysin (red).

(H) Hippocampal neuron (3 DIV) stained for arcadlin (green) and synaptophysin (red).

(I) Immunoprecipitation of N-cadherin from unstimulated (lane 1) and MECS-treated (lane 2) rat hippocampal extracts, immunoblotted for arcadlin (top), N-cadherin (middle), and β-catenin (bottom). Lane 3, control preimmune serum.

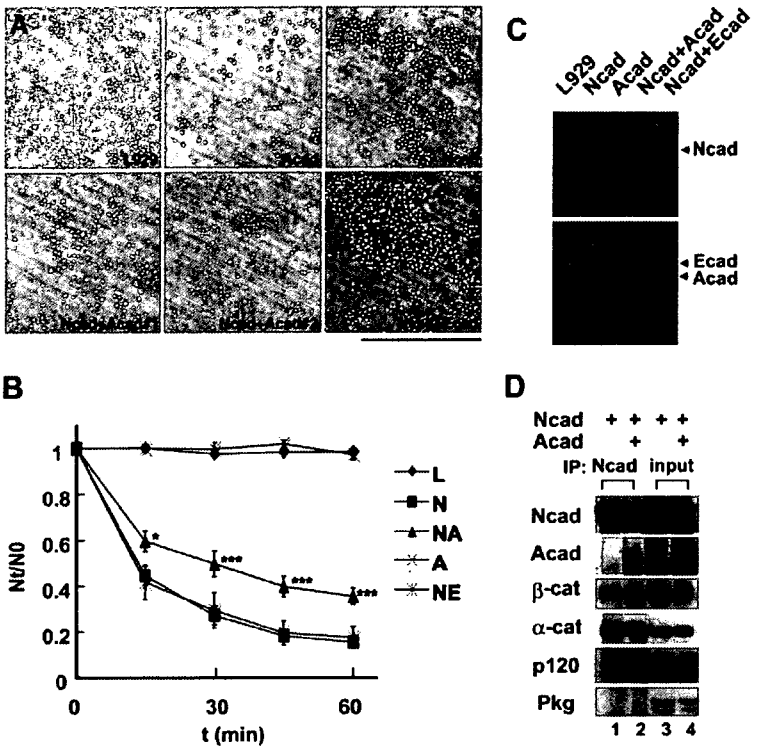

Figure 2. Arcadlin Inhibits the Adhesive Activity of N-Cadherin

(A) Cell-aggregation assay was performed using L929 cells stably transfected with *N-cadherin* (Ncad), *arcadlin* (Acad), and both (Ncad + Acad #1 and Ncad + Acad #2; two independent transfected cell lines). Scale bar, 500 μm.

(B) Adhesive activity was quantified by counting the number of aggregates (mean ± SEM) at indicated times (Nt). $^{*}p < 0.05$, $^{***}p < 0.001$, compared to Ncad.

(C) N-cadherin expression level of each cell type was examined by western blot.

(D) COS7 cells were doubly transfected with *N-cadherin* and *arcadlin* (lanes 2 and 4) or *N-cadherin* and *mock* (lanes 1 and 3), immunoprecipitated with the antibody against N-cadherin, and subjected to immunoblot (lanes 1–2). Lanes 3–4, inputs.

isolated with avidin-sepharose beads and immunoblotted for N-cadherin (Figure 3A). Membrane depolarization with KCl and elevating cAMP level, both of which induced endogenous arcadlin (Figures 1C, 1D, and 1J), resulted in significant reduction in surface N-cadherin levels (Figures 3A and 3B), whereas surface levels of neuroligin, as a control, did not change (Figures 3C and 3D).

Next, we quantified the amount of surface-associated N-cadherin microscopically. We generated a new polyclonal antibody, MT79, which recognizes the extracellular domain of N-cadherin (see Figure S1 in the Supplemental Data available with this article online). Mouse hippocampal neurons at age 14–17 days were incubated in medium containing anti-N-cadherin MT79 antibody at 4°C for 30 min. Surface-associated N-cadherins were then labeled with the secondary antibody without permeabilization of plasma membrane (Figure 3E, green). To analyze the synaptic population, we examined the N-cadherin signal that overlapped with synaptophysin (Figure 3G; synaptic versus extrasynaptic). A 33.4% ± 5.1% decrease in the mean intensity of total surface N-cadherin in the IBMX + forskolin treatment group relative to control was observed (Figures 3F and 3G). (The mean intensity of synaptophysin did not differ between groups.) The decrease in the surface N-cadherin mean intensity was observed in both the synaptic (synaptophysin-overlapping fraction) and extrasynaptic (synaptophysin-nonoverlapping fraction) populations.

(J) Immunoprecipitation of N-cadherin from cultured neurons stimulated with 25 mM KCl for 1 min and further cultured for 45–120 min, immunoblotted for arcadlin (top), N-cadherin (middle), and β-catenin (bottom). Lane 1, control preimmune serum.

(K) Immunoprecipitation of arcadlin from MECS-treated rat brain extracts, immunoblotted for cadherin-11. Left, control preimmune serum.

(L) COS7 cells were transfected with *arcadlin-EGFP* and/or *N-cadherin* and subjected to immunoprecipitation with anti-GFP serum followed by immunoblot with anti-N-cadherin antibody (top). Bottom, input. Lane 1, the lysate of *N-cadherin*-transfected cells was mixed in vitro with the lysate of *arcadlin*-transfected cells. Lane 2, arcadlin-expressing cells and N-cadherin-expressing cells were cocultured. Lane 3, *arcadlin* and *N-cadherin* were cotransfected. Lane 4, a control without transfecting *arcadlin-EGFP*. The lack of coimmunoprecipitation in lanes 1 and 2 suggested that these molecules do not interact in vitro or in *trans*, but associate laterally in the same membrane.

(M) N-cadherin mutants including wild-type (*Ncad-wt*), cytoplasmic domain deleted (*NcadΔCP*), extracellular domain deleted (*NcadΔE*), transmembrane segment alone (*Ncad-TM*), and point mutated in the middle of transmembrane region (*Ncad-L561P*, *Ncad-L561P/M562G*) were examined for the binding to full-length *arcadlin*. *N-cadherin* mutants fused with *myc*-tag were cotransfected with *arcadlin* into COS7 cells and immunoprecipitated with anti-myc antibody.

(N) Top, blot of arcadlin coimmunoprecipitated with the indicated N-cadherin mutants (lanes 1–4) or controls (lanes 5 and 6). In lane 2, abundant NcadΔCP (invisible) pushes the arcadlin band down to the lower molecular size position. Middle, arcadlin input. Bottom, immunoprecipitated N-cadherin mutants (myc probed).

(O) Top, blot of arcadlin coimmunoprecipitated with the indicated N-cadherin point mutants. Middle, arcadlin input. Bottom, immunoprecipitated N-cadherin mutants (myc probed).

Scale bars, 10 μm.

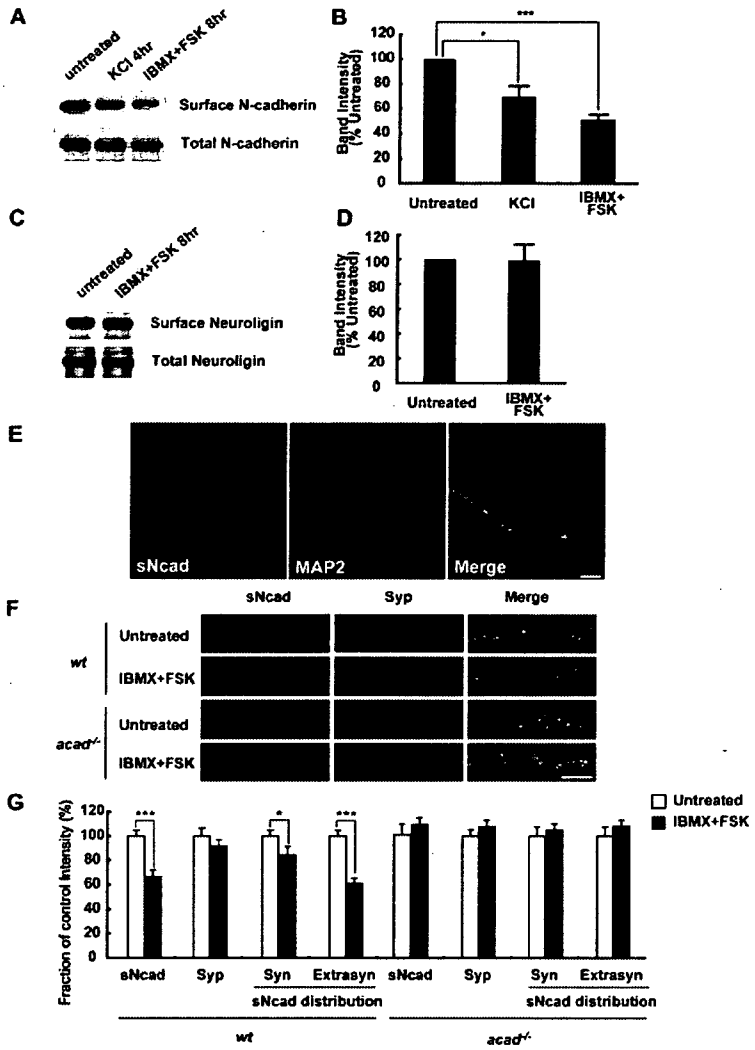

Figure 3. Depolarization or Elevated cAMP Level Increases N-Cadherin Internalization through an Arcadlin-Dependent Pathway

(A) Neuronal cell surface protein biotinylated and isolated with avidin-sepharose was immunoblotted for N-cadherin. Bottom, total protein.

(B) Densitometric quantification of surface N-cadherin levels. Surface protein levels were normalized with total protein levels and shown as proportion to the control experiment (%, mean ± SEM). n = 6.

(C) Neuronal cell surface protein was immunoblotted for neuroligin. Bottom, total protein.

(D) Densitometric quantification of surface neuroligin levels. Surface protein levels were normalized with total protein levels and shown as proportion to the control experiment (%, mean ± SEM). n = 5.

(E) Live neurons were incubated with anti-N-cadherin extracellular domain antibody (MT79) at 4°C for 30 min. Surface N-cadherin (sNcad) was labeled with Alexa-488-conjugated secondary antibody without membrane permeabilization (green). MAP2 was subsequently labeled after the permeabilization (red).

(F) Pretreatment of the neurons with IBMX and forskolin resulted in a decrease in surface N-cadherin intensity (green). Red, synaptophysin (Syp). Note that the change in surface N-cadherin intensity is not obvious in *acad/papc*$^{-/-}$ neurons.

(G) Quantification of surface N-cadherin intensity (mean ± SEM). The change in the surface N-cadherin mean intensity was observed in both the synaptophysin-overlapping fraction (Syn) and synaptophysin-nonoverlapping fraction (Extrasyn) populations. n = 40–50 dendrites from 4–5 independent experiments.

*p < 0.05, ***p < 0.001. Scale bars, 10 μm.

To show that the cAMP (IBMX + forskolin)-induced internalization of N-cadherin was indeed mediated by arcadlin, we utilized *arcadlin (acad/papc)*$^{-/-}$ mice (Yamamoto et al., 2000). The *acad*$^{-/-}$ mice were apparently normal, and the gross expression level of N-cadherin appeared the same as wild-type in brain sections and cultured neurons (data not shown). Neurons cultured from *acad*$^{-/-}$ mice extended dendrites and axons normally. The surface N-cadherin intensity of *acad*$^{-/-}$ neurons was slightly higher than that of *acad*$^{+/+}$ neurons (9.8% ± 3.6% increase in biotinylation assay, n = 5) and of *acad*$^{+/-}$ neurons (37.9 ± 1.3 [n = 100] versus 33.1 ± 0.9 [n = 100], arbitrary fluorescence units in microscopic analysis, data collected from ten independent experiments). In these *acad*$^{-/-}$ neurons, there was no significant change in the mean intensity of total surface N-cadherin in the IBMX + forskolin treatment group relative to control (Figures 3F and 3G). The data indicate that the IBMX + forskolin treatment-induced N-cadherin internalization is mediated by arcadlin.

Identification of an Isoform of TAO2 Kinase as a Signal Transducer of Arcadlin

To dissect the molecular mechanism of endocytosis of N-cadherin by arcadlin, we searched for an intracellular binding partner of arcadlin. A splice form of TAO2 kinase was cloned in a yeast two-hybrid screen using a cDNA library prepared from electroconvulsed rat hippocampi and the cytoplasmic domain of arcadlin as bait (Figure 4A and Figure S2). This isoform of TAO2 kinase (named TAO2β) of 1056 amino acids shares the common serine/threonine protein kinase catalytic domain and the MEK binding domain with the original TAO2 kinase (renamed as TAO2α hereafter) but has a unique carboxy-terminal regulatory domain that shows no apparent homology to any known protein motif (Figure 4A and Figure S2B). The mRNA portion corresponding to the C-terminal domain of TAO2α is transcribed from only one exon, whereas that encoding the TAO2β C terminus is derived partly from the same exon, and mostly from three downstream exons,